

Supermassive star formation via episodic accretion: protostellar disc instability and radiative feedback efficiency

Y. Sakurai,^{1★} E. I. Vorobyov,^{2,3} T. Hosokawa,^{1,4} N. Yoshida,^{1,5} K. Omukai⁶
and H. W. Yorke⁷

¹*Department of Physics, School of Science, University of Tokyo, Bunkyo, Tokyo 113-0033, Japan*

²*Department of Astrophysics, The University of Vienna, Vienna 1180, Austria*

³*Research Institute of Physics, Southern Federal University, Rostov-on-Don 344090, Russia*

⁴*Research Center for the Early Universe, University of Tokyo, Bunkyo, Tokyo 113-0033, Japan*

⁵*Kavli Institute for the Physics and Mathematics of the Universe (WPI), Todai Institutes for Advanced Study, the University of Tokyo, Kashiwa, Chiba 277-8583, Japan*

⁶*Astronomical Institute, Tohoku University, Sendai, Miyagi 980-8578, Japan*

⁷*Jet Propulsion Laboratory, California Institute of Technology, Pasadena, CA 91109, USA*

Accepted 2016 March 13. Received 2016 March 12; in original form 2015 November 18

ABSTRACT

The formation of supermassive stars (SMSs) is a potential pathway to seed supermassive black holes in the early universe. A critical issue for forming SMSs is stellar UV feedback, which may limit the stellar mass growth via accretion. In this paper, we study the evolution of an accreting SMS and its UV emissivity with realistic variable accretion from a circumstellar disc. First we conduct a 2D hydrodynamical simulation to follow the protostellar accretion until the stellar mass exceeds $10^4 M_{\odot}$. The disc fragments by gravitational instability, creating many clumps that migrate inward to fall on to the star. The resulting accretion history is highly time-dependent: short episodic accretion bursts are followed by longer quiescent phases. We show that the disc for the direct collapse model is more unstable and generates greater variability than normal Pop III cases. Next, we conduct a stellar evolution calculation using the obtained accretion history. Our results show that, regardless of the variable accretion, the stellar radius monotonically increases with almost constant effective temperature at $T_{\text{eff}} \simeq 5000$ K as the stellar mass increases. The resulting UV feedback is too weak to hinder accretion due to the low flux of stellar UV photons. The insensitivity of stellar evolution to variable accretion is attributed to the fact that time-scales of variability, $\lesssim 10^3$ yr, are too short to affect the stellar structure. We argue that this evolution will continue until the SMS collapses to produce a black hole by the general relativistic instability after the mass reaches $\gtrsim 10^5 M_{\odot}$.

Key words: stars: formation – galaxies: formation – cosmology: theory – early Universe.

1 INTRODUCTION

Supermassive black holes (SMBHs) with $\gtrsim 10^9 M_{\odot}$ already exist as early as at $z \gtrsim 6$ (e.g. Fan et al. 2003, 2006; Willot & Christmann 2010; Mortlock et al. 2011; Venemans et al. 2013; Wu et al. 2015). Formation of such SMBHs is a subject of intense study, since little is known about the processes leading to the accumulation of such a tremendous amount of mass within a billion years.

There are several scenarios for the early formation of the SMBHs (e.g. Volonteri 2012; Haiman 2013). A possible scenario is the so-called direct collapse model: A massive seed BH with $\sim 10^5 M_{\odot}$ (e.g. Bromm & Loeb 2003; Begelman, Volonteri & Rees 2006) increases its mass through accretion and mergers to become an

SMBH. The massive seed BH can be formed by the collapse of a supermassive star (SMS) with $\sim 10^5 M_{\odot}$ (e.g. Shibata & Shapiro 2002; Matsumoto et al. 2015). The SMS is supposed to form under special conditions which allow very rapid protostellar accretion at an average rate of $\dot{M}_* \gtrsim 0.1 M_{\odot} \text{ yr}^{-1}$. The proposed possible conditions include, e.g. gas clouds irradiated by strong photodissociating background (e.g. Sugimura, Omukai & Inoue 2014; Agarwal et al. 2015; Latif & Volonteri 2015; Latif, Schleicher & Hartwig 2015), and dense shocked gas created through the formation of protogalaxies (e.g. Inayoshi & Omukai 2012; Fernandez et al. 2014; Inayoshi, Visbal & Kashiyama 2015).

A potential obstacle for the formation of SMSs is UV feedback from the protostar itself, which might halt stellar mass growth via accretion (e.g. McKee & Tan 2008; Hosokawa et al. 2011). For normal Pop III cases with $\dot{M}_* \lesssim 0.04 M_{\odot} \text{ yr}^{-1}$, the protostar enters the so-called Kelvin–Helmholtz (KH) contraction stage at some

* E-mail: sakurai@utap.phys.s.u-tokyo.ac.jp

point. The stellar effective temperature rises as the star contracts, so that UV feedback operates with a copious flux of UV photons. However, recent studies predict a qualitatively different evolution at higher accretion rates $\gtrsim 0.04 M_{\odot} \text{ yr}^{-1}$, i.e. for the direct collapse case (e.g. Hosokawa et al. 2013; Schleicher et al. 2013); the protostar monotonically inflates with increasing stellar mass and remains at a low effective temperature $T_{\text{eff}} \simeq 5000 \text{ K}$ (named as the ‘super-giant protostar’ stage). At this low effective temperature, very few ionizing photons are emitted by the star.

The above cited work assumed constant accretion rates for simplicity. In reality, however, mass accretion occurring through self-gravitating circumstellar discs should be highly time variable. Such a disc often fragments to form clumps, some of which could be ejected, but most of which migrate inward through the disc. Accretion rates are greatly enhanced for a short time when the clump falls on to the star. The burst event is normally followed by a quiescent phase, where accretion almost ceases for a while. Numerical simulations predict that such episodic accretion commonly appears both in present-day and primordial star formation (e.g. Vorobyov & Basu 2006, 2015; Machida, Inutsuka & Matsumoto 2010; Greif et al. 2012; Smith et al. 2012; Vorobyov, DeSouza & Basu 2013a; Hosokawa et al. 2015). Although still limited, recent studies have also reported signatures of disc fragmentation for the direct collapse cases (e.g. Regan, Johansson & Haehnelt 2014; Becerra et al. 2015).

Variable accretion may allow the star to contract, as the accretion rates can temporarily fall below $\simeq 0.04 M_{\odot} \text{ yr}^{-1}$, the critical value for bloating the star. Sakurai et al. (2015, hereafter SHYY15) have calculated the stellar evolution for various episodic accretion histories, assuming periodic high and low states of accretion with a fixed mean value at $0.1 M_{\odot} \text{ yr}^{-1}$. They show that the star can contract if quiescent phases with $\dot{M}_* \ll 0.04 M_{\odot} \text{ yr}^{-1}$ continue for $\Delta t_q \gtrsim 10^3 \text{ yr} [M_*/500 M_{\odot}]^{1/2}$. Once the star contracts, the stellar effective temperature and UV emissivity rapidly rise. A longer quiescent phase results in a smaller radius and thus a larger flux of UV photons, which potentially allows an H II region to expand around the star.

SHYY15 modelled accretion histories with analytic functions to study how stellar evolution changes with different accretion histories in a controlled manner. In this paper, as a next step, we investigate stellar evolution with more realistic accretion histories. We first conduct a 2D hydrodynamical simulation following the protostellar accretion, using a central sink cell to monitor the accretion history on to the star. The resulting accretion history is highly time-dependent as the emerging circumstellar disc becomes highly gravitationally unstable. We then calculate stellar evolution using the obtained accretion history as a post process and demonstrated that the star remains in the bloated supergiant stage; the quiescent phases never last for $\Delta t_q \gtrsim 10^3 \text{ yr}$ when $M_* \gtrsim 500 M_{\odot}$.

The rest of this paper is organized as follows. In Section 2, the methods of the hydrodynamical simulation and the stellar evolution calculation are briefly explained. In Section 3, the results of the both calculations are presented. In Section 4, we discuss the implications of these results and summarize our conclusions.

2 THE NUMERICAL APPROACH

2.1 2D hydrodynamical simulations

Our model and method for numerically studying the gravitational collapse of primordial cores are presented in Vorobyov et al. (2013a). Here, we briefly review the main concepts and appropriate modifications for the formation of SMSs. We follow the evolution

of gravitationally unstable massive primordial cores from the isolated pre-stellar stage into the star and disc formation stages and terminate our simulations once about 50 per cent of the initial mass reservoir has been accreted on to the star plus disc system. Once the disc is formed, it occupies the innermost region of our numerical grid. The dynamics of both the disc and envelope are followed self-consistently on one global numerical grid, which ensures correct mass infall rates on to the star plus disc system. This is an important prerequisite for studying gravitational instability and fragmentation in young circumstellar discs at all epochs (e.g. Vorobyov & Basu 2010; Machida et al. 2010; Vorobyov et al. 2013a).

We introduce a sink cell at the inner boundary of our computational domain with a radius of $R_{\text{sc}} = 110 \text{ AU}$, and allow matter to freely flow into the sink cell. The radius of the sink cell is chosen to accommodate the maximum radius of the growing star. In the early pre-stellar phase of evolution, we monitor the mass accretion rate through the sink cell and introduce a central point-mass object (representing the forming star). In the subsequent evolution, approximately 95 per cent of the accreted material is assumed to land directly on to the star, whereas the rest is contained in the sink cell in order to keep its density equal to the mean density of the gas in the innermost 10–20 AU outside the sink cell.

We solve the usual mass and momentum transport equations written in the thin-disc approximation (see Section 3.1 for justification), using a method of finite-differences with a time-explicit, operator-split procedure similar to that described by Stone & Norman (1992) for their ZEUS-2D code. Advection is performed using the third-order piecewise parabolic scheme (Colella & Woodward 1984). The gravitational acceleration includes contributions from the central point-mass star (once formed), from material in the sink cell ($r < R_{\text{sc}}$), and from the self-gravity of the circumstellar disc and envelope.

The equations of mass and momentum transport are closed with a barotropic equation of state for the gas pressure P of the following form

$$P_k = \mathcal{K} \rho^{\gamma_k} \prod_{i=1}^{k-1} \rho_{c,i}^{\gamma_i - \gamma_{i+1}}, \quad \text{for } \rho_{c,k-1} \leq \rho < \rho_{c,k}, \quad (1)$$

where $\mathcal{K} = \mathcal{R}T/(\mu\rho^{\gamma_1-1})$, $T = 8000 \text{ K}$ is the initial gas temperature, \mathcal{R} the universal gas constant, and $\mu = 2.27$ the mean molecular weight of the primordial gas. Equation (1) is a piecewise fit to the detailed thermal and chemical evolution during direct collapse calculated by Omukai, Schneider & Haiman (2008) using a one-zone model. Whereas the solid red line in Fig. 1 portrays their exact solution, the red dashed line represents the piecewise approximation used here. The index k used in Table 1 distinguishes between the five individual components of the approximation. Also given in Table 1 for each component k are the values of the various associated polytropic indices γ_k and the associated mass and number volume densities, $\rho_{c,k}$ and $n_{c,k}$, at which transitions between k and $k+1$ occur (depicted by red dots in Fig. 1). We note that when $k=1$ the product term is unity, and the pressure reduces to $P_1 = \mathcal{K}\rho^{\gamma_1}$. Moreover, \mathcal{K} is approximately equal to the square of the initial sound speed $c_s^2 = \mathcal{R}T/\mu$, because $\gamma_1 = 0.965 \approx 1.0$.

In our simulations, the corresponding form of the barotropic relation used in the code is

$$\mathcal{P}_k = \mathcal{K} \Sigma^{\gamma_k} \prod_{i=1}^{k-1} \Sigma_{c,i}^{\gamma_i - \gamma_{i+1}}, \quad \text{for } \Sigma_{c,k-1} \leq \Sigma < \Sigma_{c,k}, \quad (2)$$

where \mathcal{P} is the vertically integrated gas pressure; the transition surface and volume mass density are related to one another through

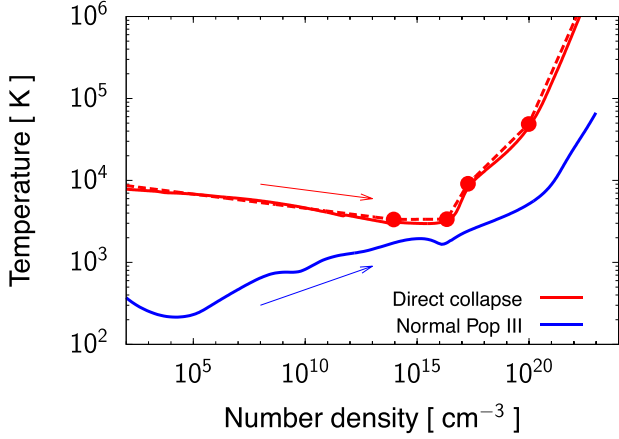


Figure 1. The temperature evolution of collapsing primordial gas as a function of the number density of hydrogen. The red line depicts the evolution of gas irradiated by a strong UV background which corresponds to the direct collapse case (fig.5a of Omukai et al. 2008, $[M/H] = -6$) considered here. The red dashed line portrays the piecewise polytropic fit used in our simulations (see the text). The blue line displays the evolution of metal-free gas in the absence of UV background (Omukai et al. 2005).

Table 1. Parameters of the barotropic relation.

k	γ_i	$\rho_{c,i}$ (g cm^{-3})	$n_{c,i}$ (cm^{-3})
1	0.965	3.38×10^{-10}	8.92×10^{13}
2	1.002	8.037×10^{-8}	2.12×10^{16}
3	1.456	7.089×10^{-7}	1.87×10^{17}
4	1.269	3.673×10^{-4}	9.69×10^{19}
5	1.614	–	–

the instantaneous local scale height Z at each point in the disc via $\Sigma_{c,i} = 2Z\rho_{c,i}$. The scale height Z is calculated assuming a local hydrostatic balance in the gravitational field of both the star and the disc (Vorobyov & Basu 2009).

The initial gas surface density Σ and angular velocity Ω profiles are similar to those that were considered in the context of normal Population III star formation (Vorobyov et al. 2013a)

$$\Sigma = \frac{r_0 \Sigma_0}{\sqrt{r^2 + r_0^2}}, \quad (3)$$

$$\Omega = 2\Omega_0 \left(\frac{r_0}{r}\right)^2 \left[\sqrt{1 + \left(\frac{r}{r_0}\right)^2} - 1 \right]. \quad (4)$$

The radial profile of Σ is an integrated form of a Bonnor–Ebert sphere, while that of Ω is the expected differential rotation profile to accompany equation (3) for a core contracting from near-uniform initial conditions (Basu 1997). The parameters $\Omega_0 = 7.22 \text{ km s}^{-1} \text{ pc}^{-1}$, $\Sigma_0 = 7.63 \text{ g cm}^{-2}$, and $r_0 = 0.154 \text{ pc}$, are the central angular velocity, central gas surface density, and the radius of a central near-constant-density plateau, respectively. They are chosen to create a gravitationally unstable core with initial mass $M_c = 26240 M_\odot$ and ratio of rotational to gravitational energy $\beta = 1.96 \times 10^{-2}$. Although the initial cloud mass is somewhat lower than that assumed for the direct-collapse model, where SMSs exceeding $10^5 M_\odot$ may finally form, this is sufficient to allow us to follow the evolution for the first $\sim 10^5$ yr of protostellar

accretion. Below we compare the resulting evolution with that discussed in Vorobyov et al. (2013a), who have followed the evolution for a similar duration but for the normal Pop III case.

Numerical simulations are run on a polar coordinate (r, ϕ) grid with 512×512 spatial zones. The radial points are logarithmically spaced, allowing improved numerical resolution of the inner grid, where the disc forms and evolves. The innermost cell outside the central sink has a radius $R_{\text{sc}} + 1.6 \text{ AU}$ and the radial and azimuthal resolution are about 14 AU at a radius of 1000 AU and 70 AU at a distance of 5000 AU. This resolution is sufficient to fulfill the Truelove criterion, which states that the local Jeans length must be resolved by at least four numerical cells (Truelove et al. 1997). Indeed, the Jeans length of a thin self-gravitating disc can be written as (Vorobyov 2013)

$$R_J = \frac{c_s^2}{G\bar{\Sigma}}. \quad (5)$$

For the mean surface density of $\bar{\Sigma} \approx 500 \text{ g cm}^{-2}$ and mean temperature $\bar{T} \approx 7500 \text{ K}$, typical for our disc at $r = 1000 - 5000 \text{ AU}$ (see Fig. 5), the corresponding Jeans length is $R_J \approx 550 \text{ AU}$ and is resolved by roughly 40 grid zones at 1000 AU and 8 grid zones at 5000 AU in each direction (r, ϕ) .

2.2 Stellar evolution calculations

We use the stellar evolution code `STELLAR` originally developed by Yorke & Bodenheimer (2008), which has been also used in SHYY15. Since the detailed description of the code is in SHYY15, we here briefly explain the main features of the code.

The code solves the basic equations of stellar evolution, including effects of mass accretion under the assumption of spherical symmetry. Nuclear reactions are considered up to helium burning (3α and $\{\text{CNO}\} + \text{He}$). Energy transport by convection is modelled by mixing length theory.

We use a grey atmosphere boundary condition for the stellar surface layer, where the accreted gas accumulates. The gas mass $\dot{M}_* \Delta t$ is added to the outermost grid cell each time step, where \dot{M}_* is the accretion rate and Δt is the stellar evolution time step. The physical quantities of the accreted gas are assumed to be the same as those in the outermost grid point. This approximates an extreme case where the accreting gas slowly approaches the star and has time to adjust thermally to the stellar surface, but is not always the case because the gas can accrete with more thermal energy. We take this into account by parametrizing the fraction of accretion luminosity deposited on to the stellar surface,

$$\eta \equiv \frac{L_{*,\text{acc}}}{L_{\text{acc}}} = L_{*,\text{acc}} \left(\frac{GM_* \dot{M}_*}{R_*} \right)^{-1}, \quad (6)$$

where $L_{*,\text{acc}}$ is the portion of accretion luminosity which contributes directly to the stellar luminosity and thus affects the stellar structure. As described in Hosokawa et al. (2013), the parameter η has a little effect on stellar evolution for high accretion rates $\gtrsim 0.1 M_\odot \text{ yr}^{-1}$ aside from the earliest accretion phases. We assume $\eta = 0.1$ in our calculations.

The initial condition is a polytrope star of $2 M_\odot$ with polytropic index $n = 1.5$, which well approximates a fully convective star. Before commencing with mass growth, the polytrope is allowed to first relax to a fully converged stellar model using `STELLAR`. The composition of the gas is assumed to be pristine with $X = 0.72$ and $Y = 0.28$. The accretion history is taken from the 2D hydrodynamical simulation (see Section 3.1).

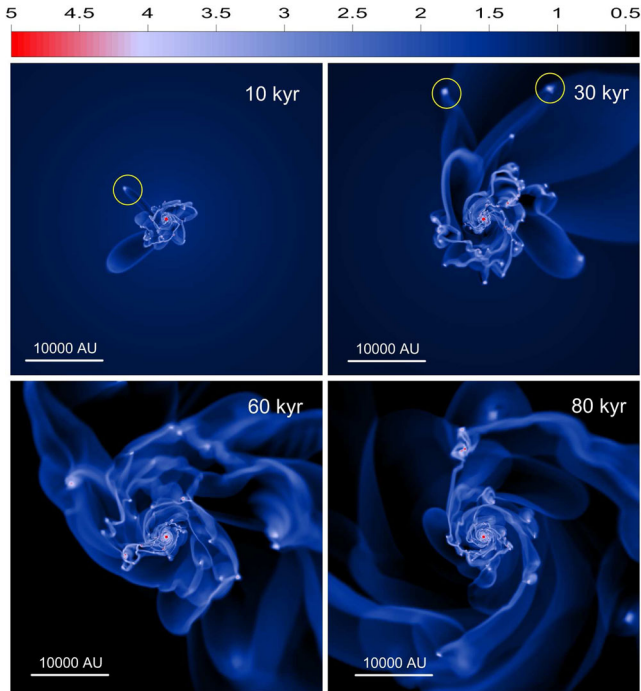


Figure 2. Images of the gas surface density in the inner $20\,000 \times 20\,000$ AU^2 box showing the evolution of the disc around the SMS star (represented schematically as a red circle in the coordinate centre). The elapsed time since the formation of the star is indicated in each panel. Yellow circles indicate the fragments that are ejected from the disc. The scale bar is in g cm^{-2} .

3 RESULTS

3.1 Episodic mass accretion with self-gravitating discs

We start by describing the evolution of a circumstellar disc formed as a result of the gravitational collapse of our massive primordial core. Fig. 2 presents the time evolution of the gas surface density in the inner $20\,000 \times 20\,000$ AU^2 box. The total computational region is about 10^2 times larger in area than shown in Fig. 2. The elapsed time since the formation of the star (schematically shown by red circles in the coordinate centre) is shown in each panel. Evidently, the disc is strongly gravitationally unstable and quickly breaks into giant spiral arcs. Gravitationally bound and pressure supported clumps form within these arcs via gravitational fragmentation.

In the absence of sink particles, tracking fragments during numerical simulations (on the fly) in grid-based codes becomes a challenging task. Therefore, we analyse the properties of the fragments in a post-process mode, using the method described in detail in Vorobyov et al. (2013a) in the context of discs around Population III stars. The algorithm is based on two conditions: the first one dictates that the fragment must be pressure supported, with a negative pressure gradient with respect to the centre of the fragment. The second condition requires that the fragment be held together by gravity, with a positive gravitational potential gradient from the deepest potential well located at the centre of the fragment.

The top panel in Fig. 3 presents the number of fragments in the disc as a function of time. The number of fragments grows with time from a few tens immediately after the formation of the central star to more than a hundred by the end of our simulations. We note that the growth is not steady but is characterized by both increases and decreases in the number of fragments, implying that fragments

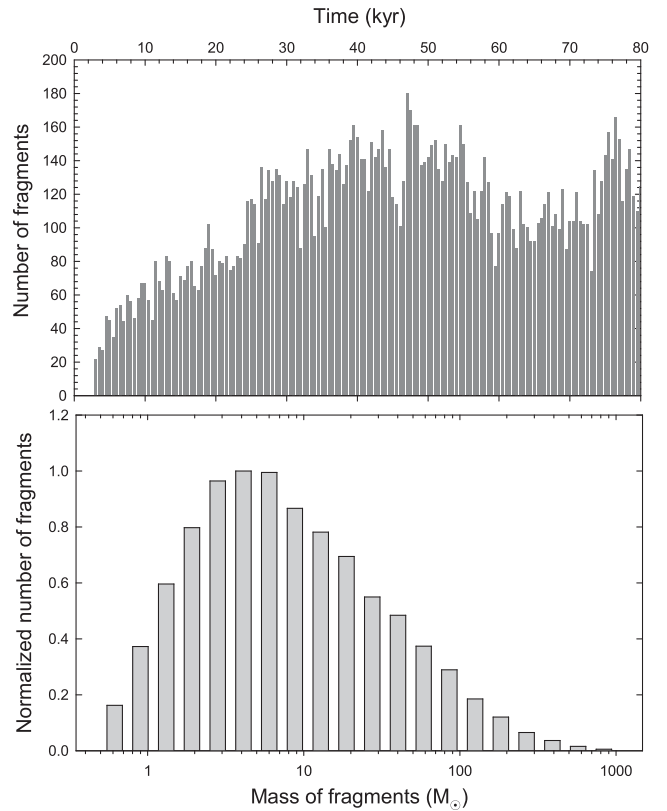


Figure 3. Top: normalized number of fragments in the disc as a function of the elapsed time since the formation of the SMS star. Bottom: the distribution function of masses of the fragments formed in the disc at all times.

can be both created and destroyed or otherwise lost by the disc. One such loss channel is accretion of the fragments on to the star caused by the loss of angular momentum due to gravitational interaction with other fragments and spiral arcs. This phenomenon is described in detail in Vorobyov & Basu (2006, 2010) in the context of present-day star formation and in Vorobyov et al. (2013a) in application to the formation of Pop III stars.

The number of fragments and the rate of their formation in our model disc is roughly a factor of 10 greater than was found in discs around present-day stars or normal Pop III stars (Vorobyov, Zakhozhay & Dunham 2013b; Vorobyov & Basu 2015). This increase in the number of fragments is a consequence of the specific temperature versus density relation typical for the direct collapse case. As the red line in Fig. 1 demonstrates, there is a wide range of gas densities in the disc, $\leq 10^{16} \text{ cm}^{-3}$, for which the gas temperature decreases as the density increases. Any compression therefore creates a positive feedback for gravitational instability – an increase in density leads to a decrease in temperature, which in turn promotes further compression and, ultimately, fragmentation. An increased number of fragments leads to much higher accretion burst activity in SMS stars than for present-day or Pop III stars (see Fig. 4 and Section 3.2 below).

The bottom panel in Fig. 3 shows the normalized distribution function of masses of the fragments. We calculate the distribution function using all fragments identified in the top panel. Since the time sampling in the top panel is 500 yr, some long-lived fragments may be duplicated so that the calculated distribution function will be

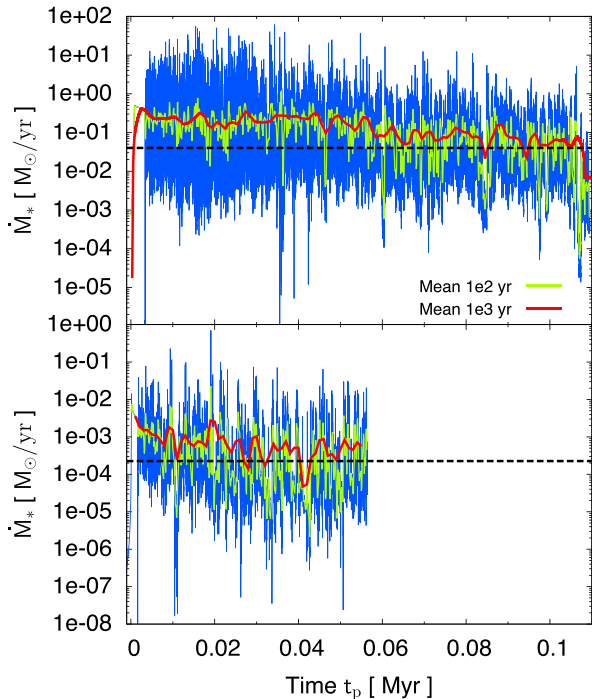


Figure 4. Comparisons of the accretion histories between the direct collapse and the normal Pop III cases. The origin of the time axis is the epoch of formation of the protostar. Top panel: the accretion history for the direct collapse case obtained by the 2D simulation. The blue line depicts the original accretion history without time averaging, and the red and green lines denote the time-averaged histories with bins of 10^3 and 100 years. Bottom panel: the accretion history for the normal Pop III case taken from Vorobyov et al. (2013a). The different colours have the same meanings as in the top panel. In each panel, the black dashed line indicates the threshold accretion rate below which the accretion is in the quiescent phase (see the text).

skewed towards long-lived fragments. The fragments vary in mass from a fraction of a solar mass to several hundred solar masses. Our simulations indicate that some of the fragments may be ejected out of the disc via multibody interactions. Several such candidates are highlighted in Fig. 2 by the yellow circles. If they can acquire sufficient velocities to escape the gravitational pull of the disc and the star, this may represent an interesting gateway for the formation of freely-floating primordial stars.

It is interesting to compare the variable accretion histories among the direct collapse case and the normal Pop III case studied by Vorobyov et al. (2013a), focusing on the duration of quiescent phases of the accretion Δt_q . In order to quantify the duration of quiescent phases, we henceforth define the quiescent phases for the direct collapse case as phases when accretion rates are below $0.04 M_\odot \text{ yr}^{-1}$, the critical rate above which the star enters the ‘supergiant’ phase (see Section 1).

For the normal Pop III case, we define the quiescent phases as phases when the accretion rate falls below one tenth of the mean value. The definition is an analogy to that for the direct collapse case: the critical accretion rate below which accretion rates become quiescent is $\sim 0.1 \times$ the mean accretion rate for the direct collapse case. In the following, we estimate Δt_q from the accretion histories for each case. In Fig. 4, the evolution of the accretion histories is shown for the direct collapse case (top panel) and the Pop III case (bottom panel). The accretion history is shown as a function

of the elapsed time since the formation of a protostar t_p . The blue line shows the original accretion history, while the red and green lines indicate the accretion histories averaged over $\Delta t_{\text{bin}} = 10^3$ and 100 yr, respectively. In each panel, the black dashed line is the threshold accretion rate \dot{M}_{th} below which the accretion is deemed quiescent. When averaging over Δt_{bin} , all variations shorter than Δt_{bin} are smoothed. Thus, the duration of quiescent phases Δt_q will be less than Δt_{bin} , if the accretion rate averaged over Δt_{bin} exceeds \dot{M}_{th} . According to the above consideration, the typical duration of quiescent phases in the direct collapse case is much smaller than 10^3 yr for $t_p \lesssim 0.06$ Myr, because the accretion rate averaged over 10^3 yr never falls below the threshold value and the accretion rate averaged over 10^2 yr seldom (and only for short periods of time $< 10^3$ yr) drops below the threshold value. The relatively long quiescent phases with $\Delta t_q \sim 10^3$ yr only appear in the late accretion stages for $t_p \gtrsim 0.06$ Myr, because of the gradual depletion of the envelope mass with time and associated weakening of gravitational fragmentation in the disc. By contrast, the quiescent phases for the normal Pop III case are much longer, $\Delta t_q \gtrsim 10^3$ yr up to the end of the calculation, because the accretion rate averaged over both 10^2 and 10^3 yr falls below the threshold value for significant periods of time.

We attribute the above difference of Δt_q to the different intervals of disc fragmentation. As previously described, the disc in the direct collapse case is more unstable than in the normal Pop III case. This means that disc fragmentation is also more frequent. A greater rate of fragments infalling on to the star results in shorter durations of quiescent phases. The key quantity for the gravitational stability of the disc is the so-called Toomre Q parameter (Toomre 1964). It is known that, for the accretion stage of star formation, the Q parameter is approximately given by $Q \sim \mathcal{O}(0.1 - 1) \times (T_{\text{disc}}/T_{\text{env}})^{3/2}$, where T_{disc} and T_{env} are the temperatures of the disc and surrounding envelope (e.g. Kratter et al. 2010; Tanaka & Omukai 2014). For $T_{\text{disc}} < T_{\text{env}}$, the disc becomes more gravitationally unstable at a smaller Q value. As can be surmised from Fig. 1, such a temperature imbalance can occur for the direct collapse case. In our 2D simulation, the number density at the boundary between the disc and envelope is $\sim 10^6$ to 10^9 cm^{-3} (see Fig. 5). Since the temperature is a decreasing function of the density for $n_{\text{H}} \lesssim 10^{16} \text{ cm}^{-3}$, the disc temperature is slightly lower than the envelope temperature. By contrast, the temperature imbalance between disc and envelope is opposite for the normal Pop III case, for which the temperature increases with increasing the density. This results in a less unstable disc, which explains the longer quiescent duration Δt_q seen in Fig. 4.

Finally, in Fig. 5 we present the azimuthally averaged gas surface and volume density as a function of distance from the star for two evolutionary times: one corresponding to the early evolution (10 kyr) and the other to the late evolution (60 kyr). Whereas low-mass fragments and spiral arcs are washed out by azimuthal averaging, the existence of massive fragments in the disc becomes apparent through the multiple short-wavelength peaks in the surface density distribution. The black circles mark the position of the disc outer edge. The positions of the black circles is calculated visually taking into account that fragments (manifested by sharp local peaks in the density profiles) form within the disc, and not within the infalling parental core. The black circles therefore separate the regions with varying (disc) and smooth (core) density profiles. We note that applying more sophisticated disc tracking mechanisms (e.g. Dunham, Vorobyov & Arce 2014) has proven difficult for our highly unstable and fragmenting discs. Moreover, some fragments may be later scattered outside the disc owing to multibody interactions, which

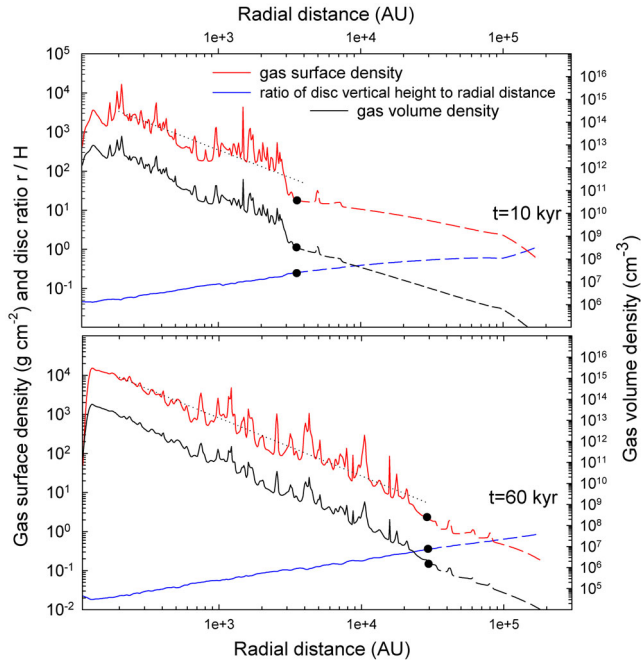


Figure 5. Azimuthally averaged gas surface and volume density profiles (red and black lines respectively) at two different evolutionary times after the formation of the star. The black circles mark the position of the disc outer edge. The black dotted lines provide the least-squares fits to the gas surface density profiles, which follow approximately an $r^{-1.5}$ law. The blue line is the ratio of the disc vertical scale height to the radial distance from the star. The outside regions of the disc are represented by the dashed lines.

would artificially increase our disc size estimates if we use the latter disc identification mechanism.

The black dotted lines are the least-squares fit to the surface density distribution in the disc. The corresponding relations at $t = 10$ kyr and $t = 60$ kyr are:

$$\Sigma \left[\frac{\text{g}}{\text{cm}^2} \right] = 10^{6.7 \pm 0.2} \left(\frac{r}{\text{AU}} \right)^{-1.4 \pm 0.06}, \quad (7)$$

$$\Sigma \left[\frac{\text{g}}{\text{cm}^2} \right] = 10^{7.4 \pm 0.1} \left(\frac{r}{\text{AU}} \right)^{-1.5 \pm 0.02}. \quad (8)$$

The disc surface density follows approximately an $r^{-1.5}$ law, also typical for self-gravitating discs around Pop III stars and in the local Universe (Vorobyov et al. 2013a). The blue lines depict the ratio of disc vertical scale height to distance from the star. Evidently, this quantity stays well below unity everywhere in the disc, justifying the use of the thin-disc approximation.

3.2 Stellar evolution under episodic accretion

We now consider the evolution of the central protostar under the variable accretion history (blue curve in the top panel of Fig. 4) obtained from the hydrodynamical simulation described in Section 3.1. Fig. 6 shows the evolution of the stellar mass and radius and the ionizing photon emissivity. As seen in the top panel of Fig. 4, the mean accretion rate approximately spans $\approx 0.1 - 0.3 M_{\odot} \text{ yr}^{-1}$, which is expected for the direct collapse model. Despite the frequent drops of the accretion rate below $0.04 M_{\odot} \text{ yr}^{-1}$, which could in principle allow stellar contraction, the protostar’s radius increases almost monotonically until the end of the calculation. The stellar radius

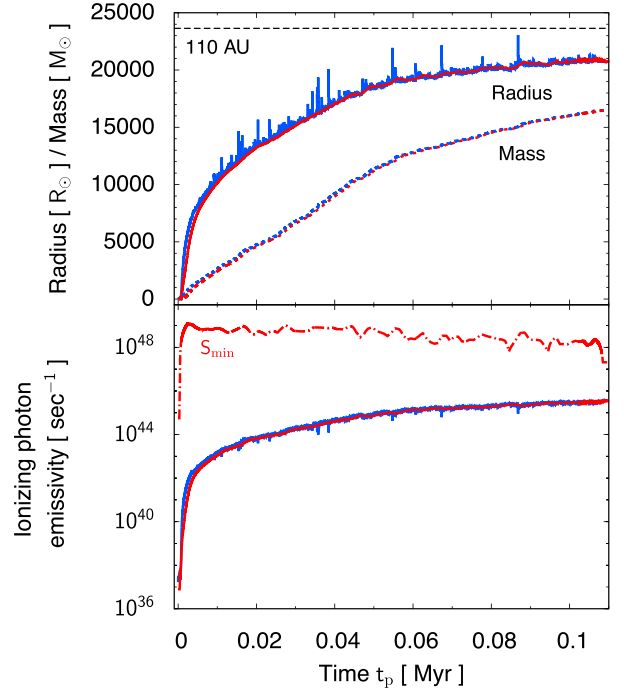


Figure 6. The time evolution of stellar mass and radius (top panel) and ionizing photon emissivity (bottom panel). The origin of the time axis is the epoch of formation of the protostar. The blue lines show the evolution without time averaging of the accretion rate (see Fig. 4). The red lines show the evolution with the accretion rates averaged with time bins 10^3 yr. The black dashed line in the top panel indicates the sink radius of 110 AU. In the bottom panel, the dot-dashed line represents the critical value above which an H II region will appear (see Section 4).

reaches 100 AU at the end of the simulation, only slightly below the sink radius of 110 AU. This evolution is similar to that for constant accretion with rates of $\gtrsim 0.1 M_{\odot} \text{ yr}^{-1}$ (e.g. fig. 1 of SHYY15). Not shown in the figure is the fact that the effective temperature remains almost constant at ≈ 5000 K due to the very sensitive temperature-dependence of H^- opacity. The ionizing photon emissivity therefore remains insufficient for creating an H II region.

SHYY15 concluded that, in order for the star to contract and leave the supergiant stage, the quiescent phase has to be longer than at least 10^3 yr for $M_* \gtrsim 500 M_{\odot}$. This explains the absence of contraction during the quiescent phases of our current simulations. SHYY15 derive the critical duration of 10^3 yr at $500 M_{\odot}$ by considering the typical KH time-scale of supergiant protostars. As shown in previous studies (e.g. Hosokawa et al. 2013), the mass distribution in the interior of the bloated protostar is highly inhomogeneous; only a surface layer with a very small fraction of the total mass largely inflates to cover most of the stellar radius. SHYY15 have thus used the KH time-scale only for the bloated surface layer $t_{\text{KH, surf}}$ [see their equation (10)], instead of the usual global definition $t_{\text{KH}} \equiv GM_*^2/R_*L_*$. SHYY15 show that the surface KH time-scale is approximately

$$t_{\text{KH, surf}} \simeq 10 t_{\text{KH}} \simeq 10^3 \text{ yr} \left(\frac{M_*}{500 M_{\odot}} \right)^{1/2}. \quad (9)$$

Since the quiescent phases found in our simulation are all shorter than this time-scale, the inflated surface layer does not have enough time to contract by radiating away thermal energy. Even for the later stage $t_p \gtrsim 0.06$ Myr when somewhat longer quiescent phases

$\Delta t_q \sim 10^3$ yr appear, the star does not contract because $t_{\text{KH, surf}}$ has also increased to $\gtrsim 10^3$ years with increasing stellar mass.

In order to evaluate the strength of UV feedback, we use the critical value of ionizing photon emissivity $S_{\text{min}} = \dot{M}/\mu m_{\text{H}}$: the value to ionize all of the atoms infalling on to the star once (see also SHYY15 and the discussion of H II region ‘squelching’ by Yorke 1986). S_{min} is the lower limit to create an H II region in spherical geometry, because, in reality, additional UV photons are needed to ionize recombined atoms. Of course, the condition of ‘squelching’ has to be fulfilled in all directions in order to entirely prevent an H II region from forming, and it is possible that a bipolar H II region could expand into the directions, from which little accretion occurs, but the extremely low UV flux ensures that the envelope can only be minimally affected by ionization. The bottom panel of Fig. 6 also shows the evolution of S_{min} , for which the accretion history averaged over 10^3 yr is used. Since the UV emissivity for the current case is always much smaller than S_{min} , no significant H II region will appear to disturb the mass accretion.

4 CONCLUSION AND DISCUSSION

We have investigated the evolution of an accreting SMS and the resulting stellar UV emissivity resulting from realistic variable mass accretion rates generated by a self-gravitating circumstellar disc. The numerical hydrodynamics simulation gives evidence of very dynamic features of the disc and protostellar accretion; the disc readily fragments and the fragments then migrate inward to fall on to the star. The resulting accretion history is highly time-dependent, characterized by a number of short episodic accretion bursts followed by somewhat longer quiescent phases. Despite the strong variability of the accretion rate, the resulting stellar evolution is quite similar to that for constant accretion rates: namely, the stellar radius increases monotonically with increasing stellar mass. The effective temperature is almost constant at $\simeq 5000$ K, a temperature at which the star produces a negligible flux of UV photons. The absence of KH contraction during quiescent accretion phases is due to their short duration, $\Delta t_q \lesssim 10^3$ yr. As shown by SHYY15, this is shorter than the local KH time-scale for the bloated stellar surface layer for $M_* \gtrsim 500 M_{\odot}$. Since the surface layer can only inefficiently radiate away thermal energy in such a short time, the star does not contract and leave the supergiant protostar stage.

In the current study, we have computed the evolution until the stellar mass reaches $\simeq 1.6 \times 10^4 M_{\odot}$ (Fig. 6). As mentioned in Section 2.1, this is mostly due to our adopted initial conditions, in particular, the limited cloud mass of $\simeq 2.6 \times 10^4 M_{\odot}$. It would be possible to simulate a longer evolution up to higher stellar masses assuming a higher initial cloud mass, but we focused on capturing the variability during the early stages of protostellar accretion, because the surface KH time-scale is shorter for lower stellar masses $t_{\text{KH, surf}} \sim 10^3 \text{ yr} [M_*/10^3 M_{\odot}]^{1/2}$.

We note that with the default sink size 110 AU, it is not until the stellar mass reaches $\simeq 1000 M_{\odot}$ that the disc first appears.¹ A test case with a 70 AU sink shows that the disc and resulting accretion variability appear earlier for $M_* \gtrsim 700 M_{\odot}$, for which Δt_q is still lower than 100 yr as in the default case. Thus, we do not currently expect stellar contraction to occur in such early stages, a fact to be

¹ The smaller the sink cell, the earlier the disc forms – disc formation occurs when the infalling material first hits its centrifugal barrier. With our chosen initial conditions, the lower angular momentum material, which hits its centrifugal barrier closer to the central star, arrives earlier.

checked by future simulations. Note that we have not adopted the smaller sink, because the radius of the inflating SMS would soon exceed the sink size.

Although the top panel of Fig. 4 shows that the duration of some quiescent phases becomes longer for $t_p \gtrsim 0.06$ Myr, we expect that this is mostly due to the gradual depletion of the accretion envelope, i.e. the stabilization of the disc (Section 3.2). For more realistic cases of direct collapse, whereby significantly more massive clouds form in so-called atomic-cooling haloes, this mass depletion would be postponed to even later times.

In order to examine if Δt_q is sufficiently short for all evolutionary stages, we estimate the duration of quiescent phases Δt_q analytically. It is expected that Δt_q is controlled by two time-scales: the fragmentation time-scale t_{frag} and the migration time-scale t_{mig} . The former is the time for a fragment to form in a gravitationally unstable disc. The latter is the time for a newly formed fragment to fall on to the central star. If $t_{\text{frag}} < t_{\text{mig}}$, we expect $t_{\text{frag}} \lesssim \Delta t_q \lesssim t_{\text{frag}} + t_{\text{mig}} \sim t_{\text{mig}}$. In this case, there will be many fragments in the disc. The minimum duration time will be realized if fragments form at regular intervals in time and migrate successively. Conversely, if $t_{\text{frag}} > t_{\text{mig}}$, the duration will be $\Delta t_q \sim t_{\text{frag}} + t_{\text{mig}} \sim t_{\text{frag}}$. The fragmentation time is estimated using the maximum growth rate ω_{max} of the gravitational instability in a linear theory (Shu 1992),

$$t_{\text{frag}} = \frac{2\pi}{\omega_{\text{max}}} = \frac{2\pi}{\Omega\sqrt{1-Q^2}} \sim \frac{2\pi}{\Omega}, \quad (10)$$

where Q is the Toomre parameter. The maximum growth rate ω_{max} is the rate for the wavenumber $k_{\text{max}} = \Omega^2/\pi G\Sigma$. In the last term, we have assumed that Q is sufficiently small. For t_{mig} , since fragments lose their angular momentum by the interaction with spiral arms in our simulation, we use the so-called Type I migration time-scale (Tanaka, Takeuchi & Ward 2002; Inayoshi & Haiman 2014),

$$t_{\text{mig}} = \frac{1}{4Cq\mu} \left(\frac{H}{r}\right)^2 \frac{2\pi}{\Omega}, \quad (11)$$

where $C = 1.160 + 2.828\alpha \sim 5.402$, $q = M_f/M_*$, $\mu = \pi\Sigma r^2/M_*$, and $H = c_s/\Omega$. The power of the surface density α is approximately 1.5 (see Fig. 5). The fragment mass M_f is estimated to be

$$M_f = \pi\lambda_{\text{max}}^2 \Sigma, \quad (12)$$

where $\lambda_{\text{max}} = 2\pi/k_{\text{max}}$. In order to assess the two time-scales, we assume that $\Omega \sim 0.5\Omega_{\text{Kep}}$, where $\Omega_{\text{Kep}} \sim \sqrt{GM(<r)/r^3}$ is the Kepler time and $M(<r)$ is the enclosed mass,

$$M(<r) = M_* + \int_{r_0}^r \Sigma 2\pi r dr. \quad (13)$$

We find the ratio $\Omega/\Omega_{\text{Kep}} \sim 0.5$ in our simulation. The lower limit of the integration r_0 is the sink radius 110 AU. For the profile of the surface density, we use $\Sigma = \Sigma_0(r/r_0)^{-1.5}$, where Σ_0 is the surface density at r_0 . We can now calculate the two time-scales as functions of radius. We find that $M(<r) \simeq M_*$ in the disk regions and thus the fragment mass and the two time-scales are

$$M_f = 14 M_{\odot} \left(\frac{\Sigma_0}{10^4 \text{ g cm}^{-2}}\right)^3 \times \left(\frac{M_*}{10^4 M_{\odot}}\right)^{-2} \left(\frac{r}{10^3 \text{ AU}}\right)^{3/2}, \quad (14)$$

$$t_{\text{frag}} = 6.3 \times 10^2 \text{ yr} \left(\frac{M_*}{10^4 M_{\odot}}\right)^{-1/2} \left(\frac{r}{10^3 \text{ AU}}\right)^{3/2}, \quad (15)$$

$$t_{\text{mig}} = 2.2 \times 10^4 \text{ yr} \left(\frac{\Sigma_0}{10^4 \text{ g cm}^{-2}} \right)^{-4} \left(\frac{T}{8000 \text{ K}} \right) \times \left(\frac{M_*}{10^4 M_\odot} \right)^{5/2} \left(\frac{r}{10^3 \text{ AU}} \right)^{1/2}. \quad (16)$$

We can see M_f is in good agreement with the typical mass $1 - 10 M_\odot$ seen in Fig. 3. The radius where $t_{\text{frag}} = t_{\text{mig}}$ is

$$r_{\text{eq}} = 3.5 \times 10^4 \text{ AU} \left(\frac{\Sigma_0}{10^4 \text{ g cm}^{-2}} \right)^{-4} \left(\frac{T}{8000 \text{ K}} \right) \times \left(\frac{M_*}{10^4 M_\odot} \right)^3. \quad (17)$$

Note that $t_{\text{frag}} < t_{\text{mig}}$ for $r < r_{\text{eq}}$. Note also that the duration Δt_q should be estimated in the disc region because fragments form in the disc. From Figs 5 and 6, we can estimate $r_{\text{eq}} = 1.8 \times 10^3 \text{ AU}$ at 10 kyr and $r_{\text{eq}} = 1.5 \times 10^4 \text{ AU}$ at 60 kyr. We see that the disc radius r_{disc} is only moderately larger than r_{eq} for these two epochs, i.e. $t_{\text{frag}} < t_{\text{mig}}$ for almost all regions of the disc. If we assume that $t_{\text{frag}} < t_{\text{mig}}$ is always realized in the disc, the minimum duration of quiescent phases $\Delta t_{q, \text{min}}$ can be estimated using t_{frag} as described above. For $M_* < 10^4 M_\odot$, we see $\Delta t_{q, \text{min}} \sim t_{\text{frag}} \lesssim 10^3 \text{ yr}$ for $r \lesssim 1000 \text{ AU}$ [see equation (15)], i.e. for the region where a large fraction of fragments form. This estimate of Δt_q is consistent with our rough estimate of Δt_q in Section 3. For $M_* > 10^4 M_\odot$, we expect that Δt_q becomes shorter since $t_{\text{frag}} \propto M_*^{-1/2}$. The duration Δt_q can become longer if the disc becomes less unstable and Q becomes larger [equation (10)]. In fact, in our simulation the accretion rate gradually diminishes for $M_* \gtrsim 10^4 M_\odot$ (Fig. 4) and the disc may indeed become more stable. However, if we used a heavier initial cloud mass as the initial condition, there will be ample gas supply. In this case, the disc will continue to be unstable for $M_* \gtrsim 10^4 M_\odot$ and it is unlikely that the assumption $Q \ll 1$ breaks down. Therefore, we do not expect significant stellar contraction for any SMS mass, until the stellar mass exceeds $\sim 10^5 M_\odot$. At this point, the SMS is expected to collapse and produce a massive BH via the general relativistic instability.

It is often suspected that fragments formed in the disc may become zero-age main sequence (ZAMS) stars before destruction. In this case, the stars will emit UV photons and UV feedback can operate. Several studies consider fragmentation and clump migration in a disc around a SMS using analytical models (e.g. Lodato & Natarajan 2006; Inayoshi & Haiman 2014; Latif & Schleicher 2015). Inayoshi & Haiman (2014) and Latif & Schleicher (2015) argue that fragments do not become ZAMS stars before they fall on to the central star for $M_* \lesssim 10^4 M_\odot$, since the migration time-scale is shorter than the KH time-scale of the fragments $t_{\text{KH}} = GM_f^2/R_f L_f$, where R_f is a radius of fragments and L_f is luminosity of them. Conversely, for $M_* \gtrsim 10^4 M_\odot$, the groups concluded that fragments can become ZAMS stars. In order to assess whether UV feedback from fragments is plausible, we estimate the KH time-scale of the fragments. As seen in fig. 4 of Hosokawa & Omukai (2009), the KH time t_{KH} is comparable to or larger than the accretion time-scale $t_{\text{acc}} = M_f/\dot{M}_f$ before the star reaches ZAMS if $\dot{M}_f \lesssim 10^{-2} M_\odot \text{ yr}^{-1}$, where \dot{M}_f is the accretion rate of fragments. We then estimate the KH time (Inayoshi & Haiman 2014)

$$t_{\text{KH}} \gtrsim 10^4 \text{ yr} \left(\frac{M_f}{30 M_\odot} \right) \left(\frac{\dot{M}_f}{0.003 M_\odot \text{ yr}^{-1}} \right)^{-1}. \quad (18)$$

For the accretion rate of fragments \dot{M}_f , we use

$$\dot{M}_f = \frac{3}{2} \Sigma \Omega (f_H R_H)^2, \quad (19)$$

where $R_H = r(M_f/3M_*)^{1/3}$ is the Hill radius and f_H is $\mathcal{O}(1)$ (Goodman & Tan 2004). We set $f_H = 1$. We derive the approximate form

$$\dot{M}_f = 3.6 \times 10^{-3} M_\odot \text{ yr}^{-1} \left(\frac{\Sigma_0}{10^4 \text{ g cm}^{-2}} \right)^3 \times \left(\frac{M_*}{10^4 M_\odot} \right)^{-5/6} \left(\frac{r}{100 \text{ AU}} \right)^{-1/3}. \quad (20)$$

Using equations (14) and (20), the KH time becomes

$$t_{\text{KH}} \gtrsim 1.7 \times 10^2 \text{ yr} \left(\frac{\Sigma_0}{10^4 \text{ g cm}^{-2}} \right)^{-1/3} \times \left(\frac{M_*}{10^4 M_\odot} \right)^{-3/2}. \quad (21)$$

The ratio of t_{mig} to t_{KH} is

$$\frac{t_{\text{mig}}}{t_{\text{KH}}} \lesssim 5.9 \left(\frac{\Sigma_0}{10^4 \text{ g cm}^{-2}} \right)^{-4} \left(\frac{M_*}{10^4 M_\odot} \right)^3 \times \left(\frac{r}{10^3 \text{ AU}} \right)^{-1} \left(\frac{T}{8000 \text{ K}} \right). \quad (22)$$

Because of the dependence of the ratio on M_* , for t_{mig} to be comparable to t_{KH} , M_* needs to be at least $\gtrsim 10^4 M_\odot$. This discussion is then roughly consistent with the models of the other groups: for $M_* \lesssim 10^4 M_\odot$, UV feedback from fragments will not be effective. However, there are other mechanisms to be considered in order to investigate the fate of the fragments. The mechanisms include tidal disruption of fragments by the central star, interactions between fragments and possibly ejection. In order to assess the impact of UV feedback from fragments more correctly, it is necessary to conduct 3D simulations including radiation in future studies.

Finally, we note possible dimensional effects in a realistic three-dimensional disc. Fragments formed in a 3D disc can interact with the central star and with other fragments in a complex manner. Unlike in our 2D simulations where the fragments simply move either inward or outward, dynamical interaction of the fragments would induce more stochastic accretion that presented here. However, the resulting dynamics in our 2D simulations is overall similar to that in 3D simulations, wherein most fragments migrate towards the star (Cha & Nayakshin 2011; Machida, Inutsuka & Matsumoto 2011; Greif et al. 2012). Three dimensional simulations will be needed to study explicitly the impact of fragmentation to SMS formation.

ACKNOWLEDGEMENTS

YS thanks the support from Advanced Leading Graduate Course for Photon Science. EIV acknowledges the support from the Russian Ministry of Education and Science Grant 3.961.2014/K. This work was financially supported by Grant-in-Aid for JSPS Fellows (15H00776: YS), by JSPS-OEAD short-term research grant #RC (21402003: EIV), and by the Grants-in-Aid for Basic Research by the Ministry of Education, Science and Culture of Japan (25800102, 15H00776: TH, 25287040: KO, 25287050: NY). Portions of this work were conducted at the Jet Propulsion Laboratory, California Institute of Technology, operating under a contract with the National Aeronautics and Space Administration (NASA). Numerical simulations were done on the Vienna Scientific Cluster (VSC-2),

Atlantic Computational Excellence Network (ACEnet), and Shared Hierarchical Academic Research Computing Network (SHARC-NET). The stellar evolution calculations were partly conducted on a PC cluster at the Center for Computational Astrophysics, National Astronomical Observatory of Japan.

REFERENCES

- Agarwal B., Smith B., Glover S., Natarajan P., Khochfar S., 2015, preprint ([arXiv:1504.04042](https://arxiv.org/abs/1504.04042))
- Basu S., 1997, *ApJ*, 485, 240
- Becerra F., Greif T. H., Springel V., Hernquist L. E., 2015, *MNRAS*, 446, 2380
- Begelman M. C., Volonteri M., Rees M. J., 2006, *MNRAS*, 370, 289
- Bromm V., Loeb A., 2003, *ApJ*, 596, 34
- Cha S.-H., Nayakshin S., 2011, *MNRAS*, 415, 3319
- Colella P., Woodward P. R., 1984, *J. Comput. Phys.*, 54, 174
- Dunham M. M., Vorobyov E. I., Arce H. G., 2014, *MNRAS*, 444, 887
- Fan X., Strauss M. A., Schneider D. P., Becker R. H., White R. L., Haiman Z., Gregg M., Pentericci L., 2003, *AJ*, 125, 1649
- Fan X., Strauss M. A., Richards G. T., Hennawi J. F., Becker R. H., White R. L., Diamond-Stanic A. M., 2006, *AJ*, 131, 1203
- Fernandez R., Bryan G. L., Haiman Z., Li M., 2014, *MNRAS*, 439, 3798
- Goodman J., Tan J. C., 2004, *ApJ*, 608, 108
- Greif T. H., Bromm V., Clark P. C., Glover S. C. O., Smith R. J., Klessen R. S., Yoshida N., Springel V., 2012, *MNRAS*, 424, 399
- Haiman Z., 2013, in Wiklind T., Mobasher B., Bromm V., eds, *Astrophysics and Space Science Library*, Vol. 396, *The First Galaxies*. Springer-Verlag, Berlin, p. 293
- Hosokawa T., Omukai K., 2009, *ApJ*, 691, 823
- Hosokawa T., Omukai K., Yoshida N., Yorke H. W., 2011, *Science*, 334, 1250
- Hosokawa T., Yorke H. W., Inayoshi K., Omukai K., Yoshida N., 2013, *ApJ*, 778, 178
- Hosokawa T., Hirano S., Kuiper R., Yorke H. W., Omukai K., Yoshida N., 2015, preprint ([arXiv:1510.01407](https://arxiv.org/abs/1510.01407))
- Inayoshi K., Haiman Z., 2014, *MNRAS*, 445, 1549
- Inayoshi K., Omukai K., 2012, *MNRAS*, 422, 2539
- Inayoshi K., Visbal E., Kashiyama K., 2015, preprint ([arXiv:1504.00676](https://arxiv.org/abs/1504.00676))
- Kratter K. M., Matzner C. D., Krumholz M. R., Klein R. I., 2010, *ApJ*, 708, 1585
- Latif M. A., Schleicher D. R. G., 2015, *A&A*, 578, A118
- Latif M. A., Volonteri M., 2015, *MNRAS*, 452, 1026
- Latif M. A., Schleicher D. R. G., Hartwig T., 2015, preprint ([arXiv:1510.02788](https://arxiv.org/abs/1510.02788))
- Lodato G., Natarajan P., 2006, *MNRAS*, 371, 1813
- Machida M. N., Inutsuka S.-i., Matsumoto T., 2010, *ApJ*, 724, 1006
- Machida M. N., Inutsuka S.-i., Matsumoto T., 2011, *ApJ*, 729, 42
- Matsumoto T., Nakauchi D., Ioka K., Heger A., Nakamura T., 2015, *ApJ*, 810, 64
- McKee C. F., Tan J. C., 2008, *ApJ*, 681, 771
- Mortlock D. J. et al., 2011, *Nature*, 474, 616
- Omukai K., Tsuribe T., Schneider R., Ferrara A., 2005, *ApJ*, 626, 627
- Omukai K., Schneider R., Haiman Z., 2008, *ApJ*, 686, 801
- Regan J. A., Johansson P. H., Haehnelt M. G., 2014, *MNRAS*, 439, 1160
- Sakurai Y., Hosokawa T., Yoshida N., Yorke H. W., 2015, *MNRAS*, 452, 755 (SHYY15)
- Schleicher D. R. G., Palla F., Ferrara A., Galli D., Latif M., 2013, *A&A*, 558, A59
- Shibata M., Shapiro S. L., 2002, *ApJ*, 572, L39
- Shu F. H., 1992, *Physics of Astrophysics*, Vol. 2. University Science Books, Sausalito, CA
- Smith R. J., Hosokawa T., Omukai K., Glover S. C. O., Klessen R. S., 2012, *MNRAS*, 424, 457
- Stone J. M., Norman M. L., 1992, *ApJS*, 80, 753
- Sugimura K., Omukai K., Inoue A. K., 2014, *MNRAS*, 445, 544
- Tanaka K. E. I., Omukai K., 2014, *MNRAS*, 439, 1884
- Tanaka H., Takeuchi T., Ward W. R., 2002, *ApJ*, 565, 1257
- Toomre A., 1964, *ApJ*, 139, 1217
- Truelove J. K., Klein R. I., McKee C. F., Holliman, II J. H., Howell L. H., Greenough J. A., 1997, *ApJ*, 489, L179
- Venemans B. P. et al., 2013, *ApJ*, 779, 24
- Volonteri M., 2012, *Science*, 337, 544
- Vorobyov E. I., 2013, *A&A*, 552, A129
- Vorobyov E. I., Basu S., 2006, *ApJ*, 650, 956
- Vorobyov E. I., Basu S., 2009, *MNRAS*, 393, 822
- Vorobyov E. I., Basu S., 2010, *ApJ*, 719, 1896
- Vorobyov E. I., Basu S., 2015, *ApJ*, 805, 115
- Vorobyov E. I., DeSouza A. L., Basu S., 2013a, *ApJ*, 768, 131
- Vorobyov E. I., Zakhzhay O. V., Dunham M. M., 2013b, *MNRAS*, 433, 3256
- Willot M., Christmann M., 2010, *Nat. Chem.*, 2, 519
- Wu X.-B. et al., 2015, *Nature*, 518, 512
- Yorke H. W., 1986, *ARA&A*, 24, 49
- Yorke H. W., Bodenheimer P., 2008, in Beuther H., Linz H., Henning T., eds, *ASP Conf. Ser. Vol. 387, Massive Star Formation: Observations Confront Theory*. Astron. Soc. Pac., San Francisco, p. 189

This paper has been typeset from a $\text{\TeX}/\text{\LaTeX}$ file prepared by the author.